Nanotechnology Overview

清華大學物理系 果尚志
Shangjr Gwo
Department of Physics
National Tsing-Hua University
Hsinchu 300, Taiwan
E-mail: gwo@phys.nthu.edu.tw

Some History

The Great Pyramid at Giza

Pharaoh Khufu (2585-2560 B.C.)

Base: >13 acres
Height: 450 feet/137.2 meters

The Great Wall of China

Over 50,000 km

Building Period:
9th Century B.C. (Zhou)
to 17th Century (Ming)

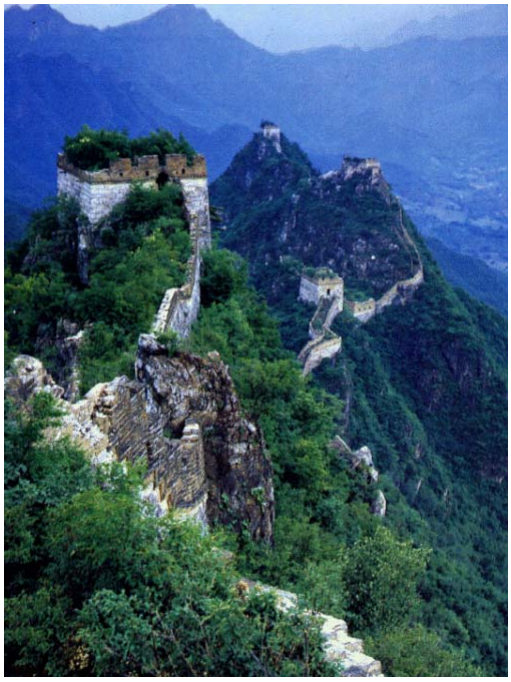

Apollo 11 Journey to the Moon (1969)

The distance from Earth to Moon: 384,400 km (240,250 miles)

R. P. Feynman
"There is plenty of room at the bottom" (1959)

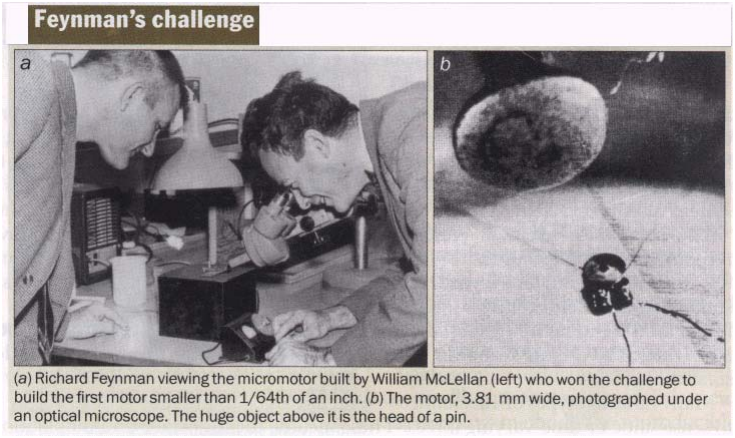

(a) Richard Feynman viewing the micromotor built by William McLellan (left) who won the challenge to build the first motor smaller than 1/64th of an inch. (b) The motor, 3.81 mm wide, photographed under an optical microscope. The huge object above it is the head of a pin.

「一尺之棰，日取其半，萬世不竭。」

公孫龍（約西元前320－350）—《莊子》雜篇「天下」

National Palace Museum, Taipei, Taiwan

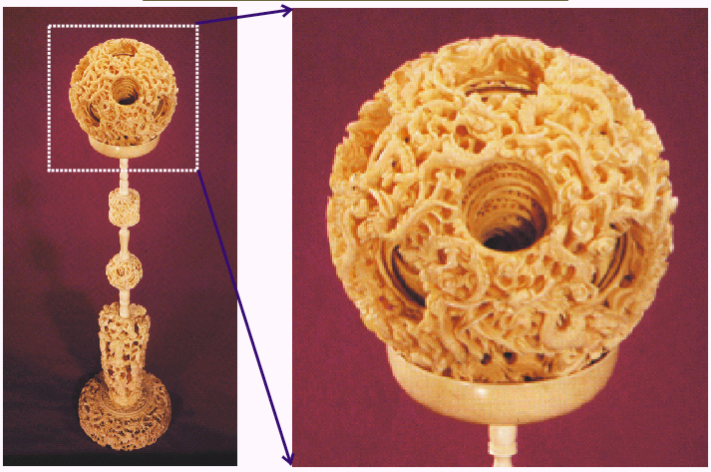

雕象牙 透花雲龍紋套球 (清代) Ivory Sculpture (Ch'ing Dynasty)

Scanometric DNA Array Detection with Nanoparticle Probes

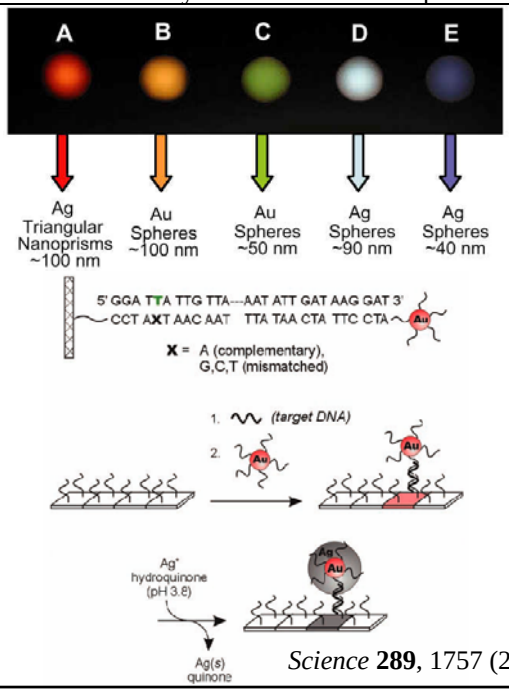

Science **289**, 1757 (2000)

Red gold. Stained-glass window in Milan Cathedral, Italy, made by Niccolo da Varallo between 1480 and 1486, showing the birth of St. Eligius, patron saint of gold-smiths. The red colors are due to colloidal gold.

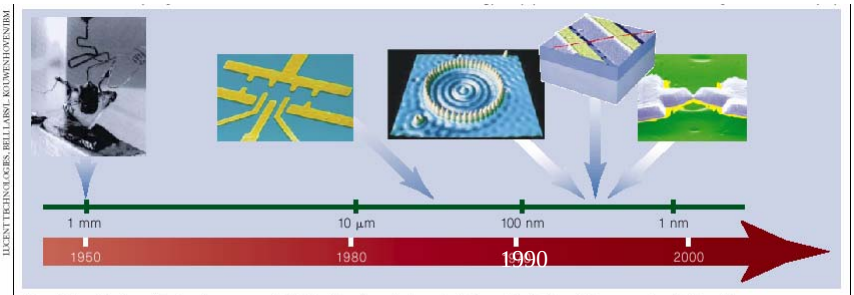

Figure 1 **The shrinkage of electronic components. The length scale reached by technology has dropped steadily from the millimetre scale of the early 1950s to the present-day atomic scale. The representative devices, from left to right, are: the first transistor, a quantum-dot turnstile, a copper 'quantum corral', a carbon-nanotube transistor, and the latest — a one-atom point contact.**

NATURE | VOL 394 | 9 JULY 1998

Worldwide Budget for Nanotechnology

- US National Nanotechnology Initiative
  Annual budget: $423 million in 2001
- Japan
  Annual budget: $396 million in 2001
- Europe…

Why? Fiction or Reality?

奈米科技中的核心技術

- 奈米材料(奈米微粒、奈米管、奈米棒、奈米電纜等)
- 奈米製程(微影、蝕刻、成長、自我組裝等)
- 奈米結構(人造原子、量子點、量子線、量子井等)
- 奈米物性測量(光性、電性、磁性、力學性質、熱學性質、觸媒作用等)
- 奈米操控技術

The most needed ingredient in nanotechnology:
A missing link between nm, μm, mm, to cm worlds

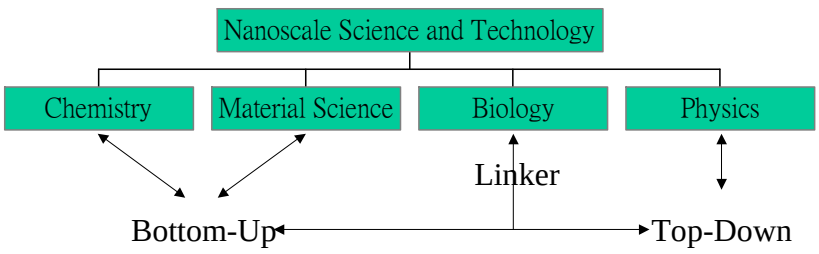

Biological Scaling Laws

Weight in proportion to L^3
Strength in proportions to L^2

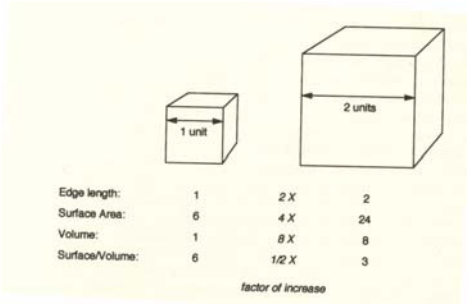

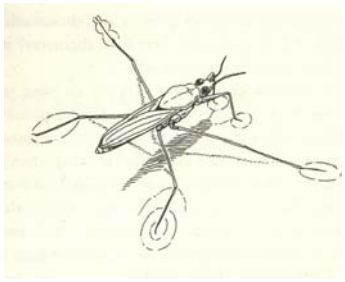

FIGURE 41.24 The image of a Mediterranean fruit fly produced by a scanning electron microscope has a great depth of field.

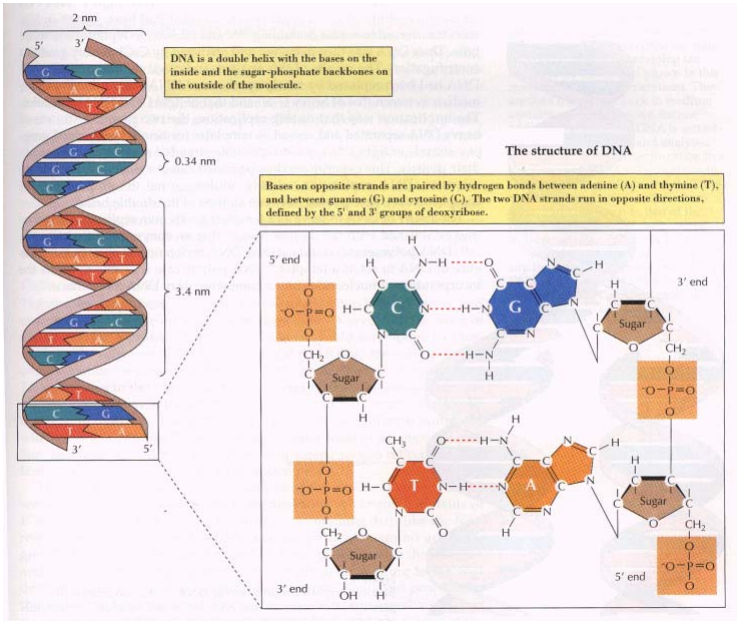
2 nm
5′
3′
DNA is a double helix with the bases on the inside and the sugar-phosphate backbones on the outside of the molecule.
0.34 nm
3.4 nm
The structure of DNA
Bases on opposite strands are paired by hydrogen bonds between adenine (A) and thymine (T), and between guanine (G) and cytosine (C). The two DNA strands run in opposite directions, defined by the 5′ and 3′ groups of deoxyribose.
5′ end
3′ end
Sugar
3′ end
5′ end
OH

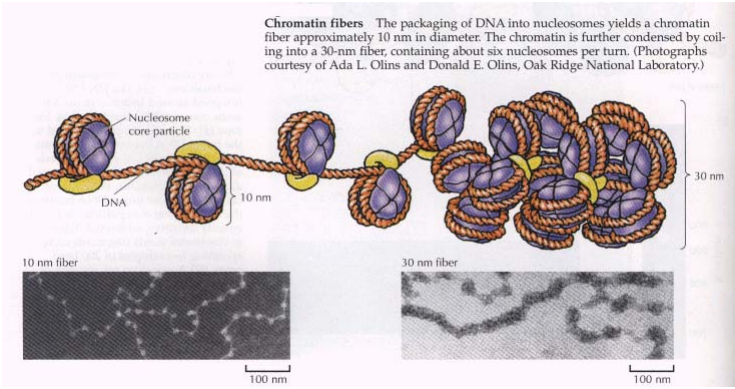
Chromatin fibers The packaging of DNA into nucleosomes yields a chromatin fiber approximately 10 nm in diameter. The chromatin is further condensed by coiling into a 30-nm fiber, containing about six nucleosomes per turn. (Photographs courtesy of Ada L. Olins and Donald E. Olins, Oak Ridge National Laboratory.)
Nucleosome core particle
DNA
10 nm
30 nm
10 nm fiber
30 nm fiber
100 nm
100 nm

Examples of Micromachined Actuators

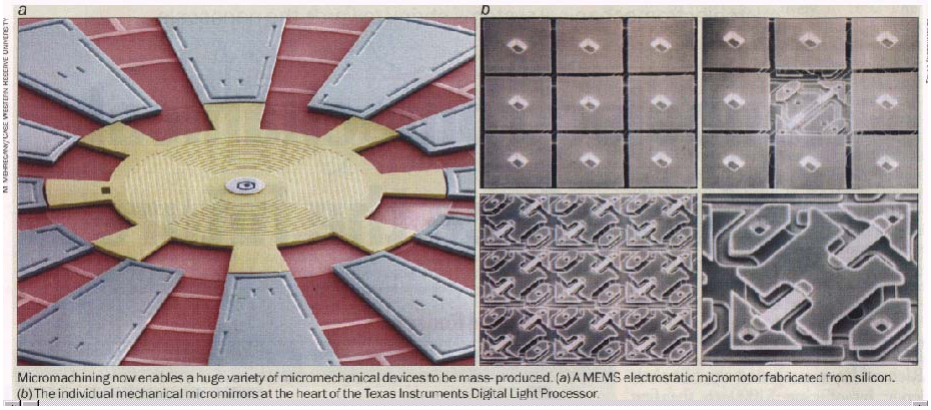

Micromachining now enables a huge variety of micromechanical devices to be mass-produced. (a) A MEMS electrostatic micromotor fabricated from silicon. (b) The individual mechanical micromirrors at the heart of the Texas Instruments Digital Light Processor.

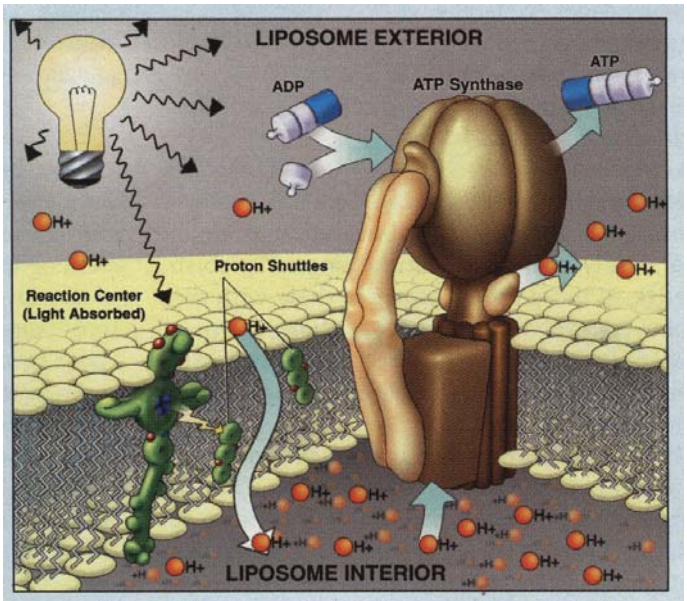

Power plant. Molecules embedded in a membrane use light to generate energy-rich ATP.

Biomolecular Motor

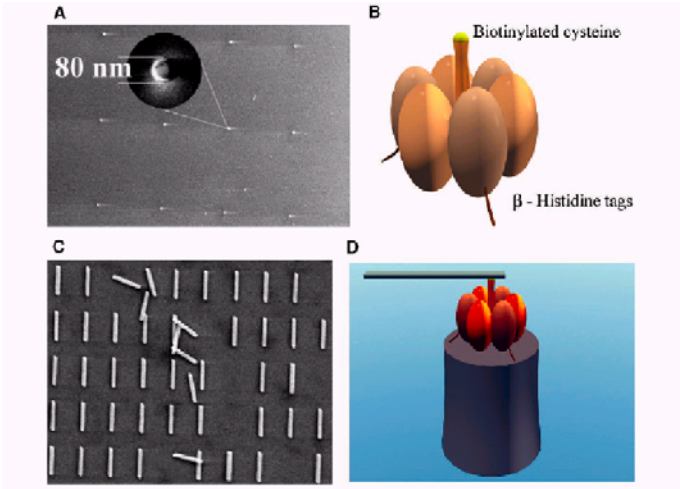

Fig. 1. Schematic diagram of the F_1-ATPase biomolecular motor–powered nanomechanical device. The device consisted of **(A)** a Ni post (height 200 nm, diameter 80 nm), **(B)** the F_1-ATPase biomolecular motor, and **(C)** a nanopropeller (length 750 to 1400 nm, diameter 150 nm). The device **(D)** was assembled using sequential additions of individual components and differential attachment chemistries.

Nanobiotechnology Center, Cornell University

A Example of Sensor: *Torsion Balance*
Detection mode: deflection (static) or vibration (dynamic)

Charles A. Coulomb
(1736–1806).

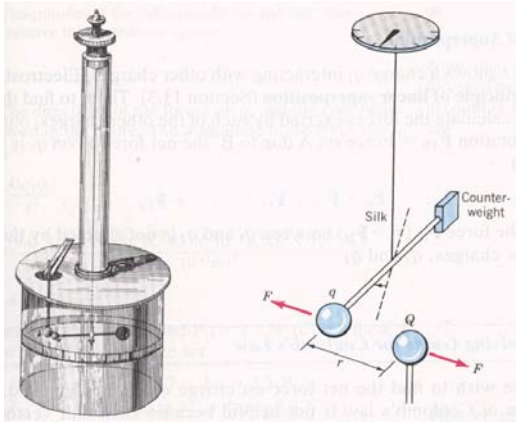

1785

Nanoelectromechanical Systems (NEMS)

- **Fast response (ω_0/Q)**
- **Wide detection range (ω_0)**
- **High sensitivity (small mass and high Q)**
- **Localized spatial response**
- **Low dissipation (Q)**
- **Ultra-low operation power**
- **Compatible to microelectronics**

$\omega_0=(k_{eff}/m_{eff})^{1/2}$
m_{eff} **in proportion to** l^3
k_{eff} **in proportion to** l
ω_0 **in proportion to** $1/l$
m_{eff} **~ a few attograms** (10^{-18} **g)**
cross section ~ 10 nm
ω_0 **~ >10 GHz** (10^{10} **Hz)**

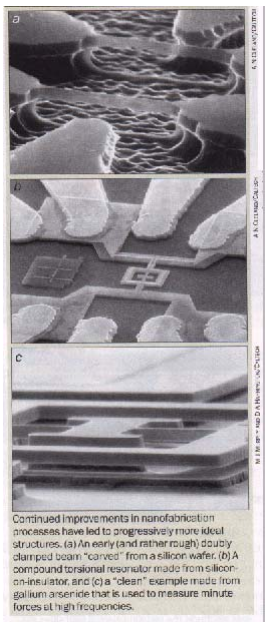

Continued improvements in nanofabrication processes have led to progressively more ideal structures. (a) An early (and rather rough) doubly clamped beam "carved" from a silicon wafer. (b) A compound torsional resonator made from silicon-on-insulator, and (c) a "clean" example made from gallium arsenide that is used to measure minute forces at high frequencies.

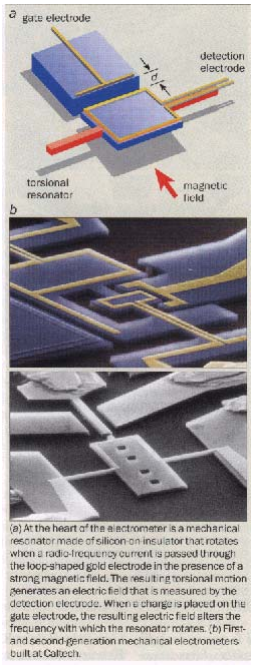

(a) At the heart of the electrometer is a mechanical resonator made of silicon-on-insulator that rotates when a radio-frequency current is passed through the loop-shaped gold electrode in the presence of a strong magnetic field. The resulting torsional motion generates an electric field that is measured by the detection electrode. When a charge is placed on the gate electrode, the resulting electric field alters the frequency with which the resonator rotates. (b) First- and second-generation mechanical electrometers built at Caltech.

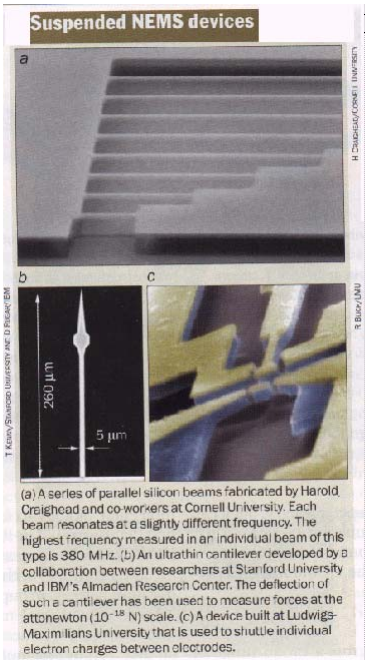

(a) A series of parallel silicon beams fabricated by Harold Craighead and co-workers at Cornell University. Each beam resonates at a slightly different frequency. The highest frequency measured in an individual beam of this type is 380 MHz. (b) An ultrathin cantilever developed by a collaboration between researchers at Stanford University and IBM's Almaden Research Center. The deflection of such a cantilever has been used to measure forces at the attonewton (10^{-18} N) scale. (c) A device built at Ludwig-Maximilians University that is used to shuttle individual electron charges between electrodes.

NEMS meet quantum mechanics

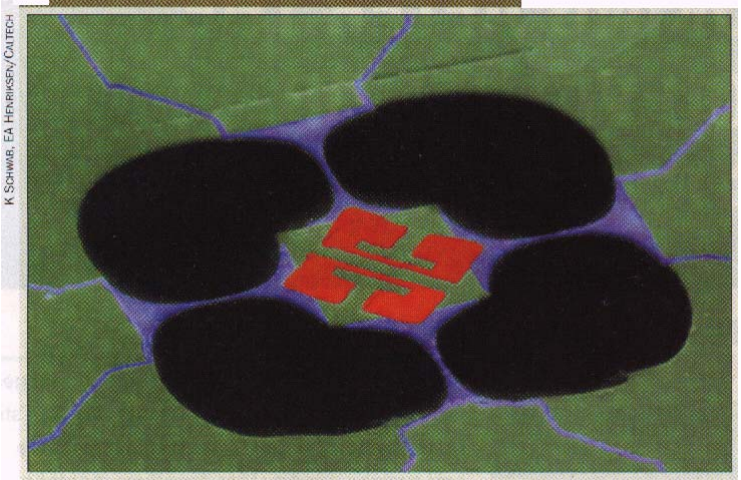

K. Schwab, E.A. Henriksen/Caltech

A suspended mesoscopic thermal transport devices that recently enabled the first measurement of the quantum of thermal conductance. The device is surrounded by thin phonon waveguides and consists of a thin silicon-nitride membrane at the centre that is supported by the thin phonon waveguides.

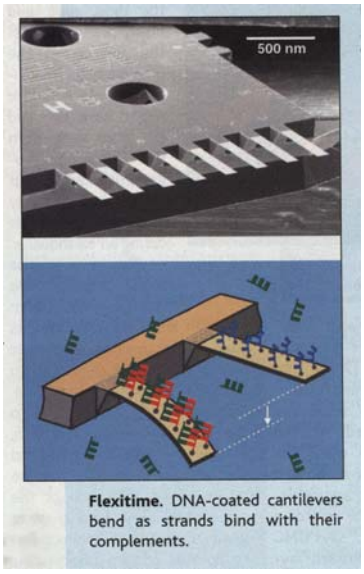

Flexitime. DNA-coated cantilevers bend as strands bind with their complements.

J. Gimzewski, IBM Zurich

Scanning Probe Concept:
Eye and Hand
in the Nanometer-Scale World

Inventors:
G. Binning and H. Rohrer

Examples:
STM
AFM
MFM
EFM
SCM
SGM
etc.

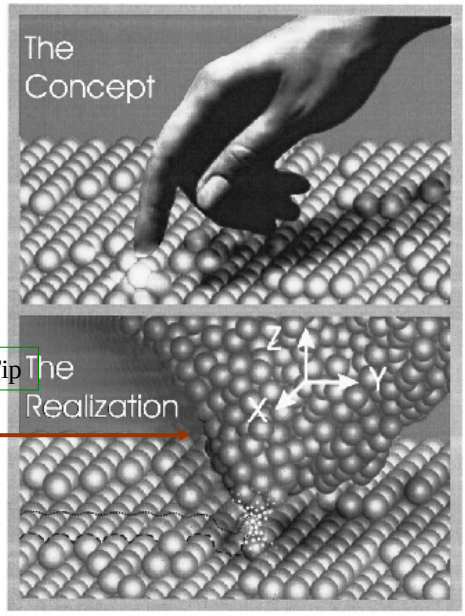

G. Binnig and and H. Rohrer in *Rev. of Mod. Phys.*, vol. 71, ppS324-S330 (March, 1999).

An earlier version of STM by Binnig and Rohrer (1982)

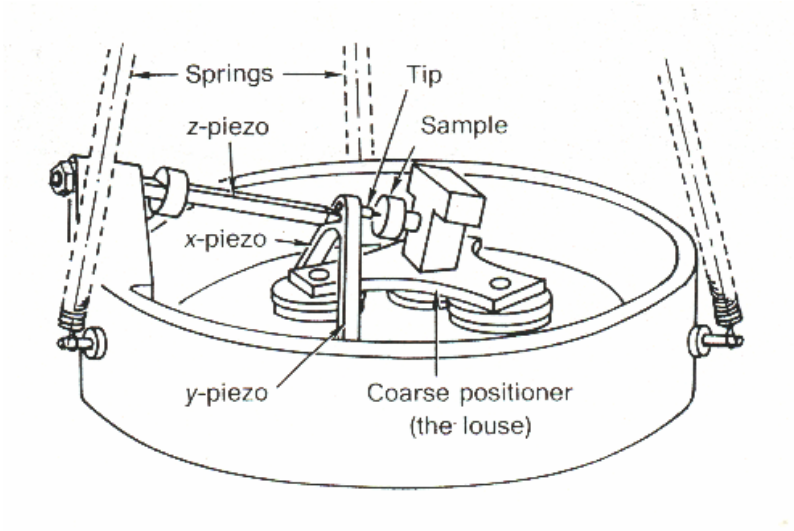

Scanning Tunneling Microscope

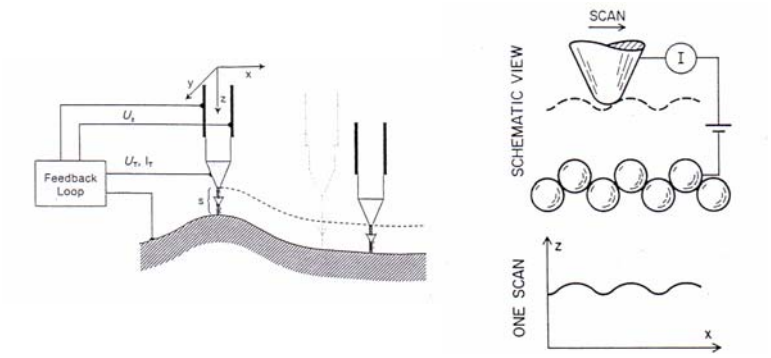

Tunneling Energy Diagram

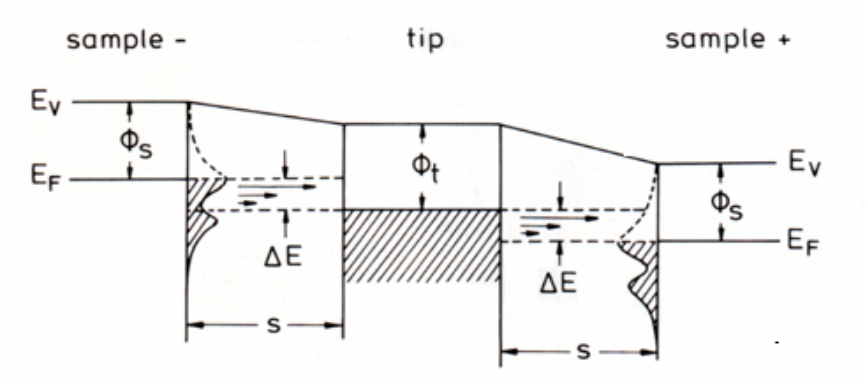

Quantum Corral

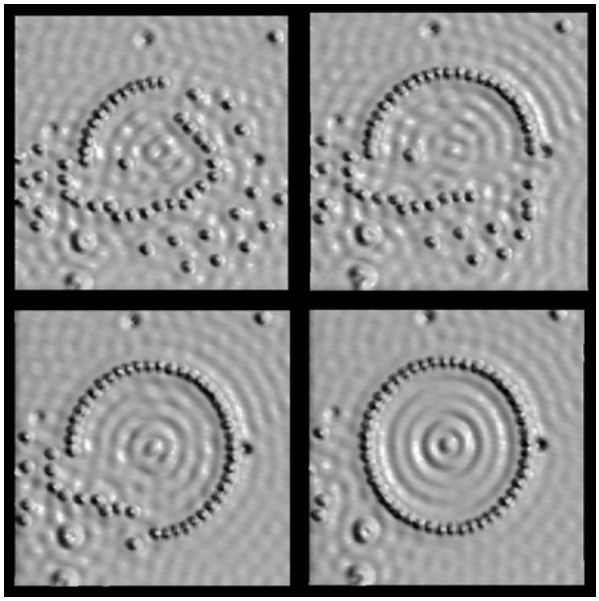

Don Eigler
IBM Almaden

Quantum Mirage

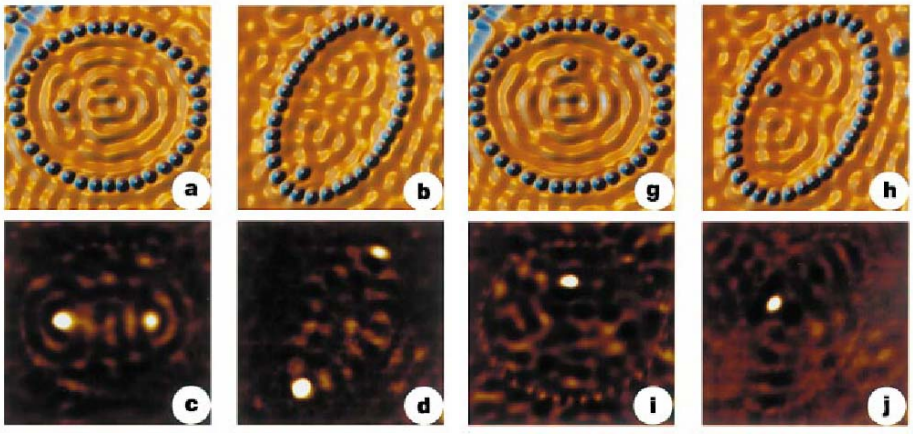

***Nature*, H. C. Manoharan *et al*., Vol. 403, p. 512 (2000)**

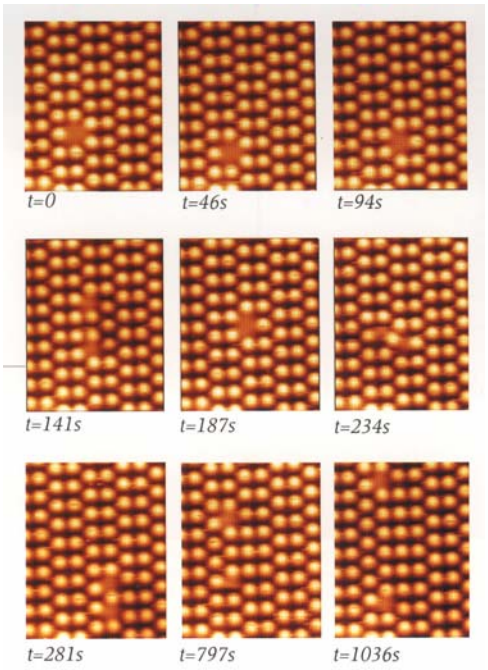

Vacancy Motion on Ge(111)-*c*(2x8)
(France's Commission for Atomic Energy)

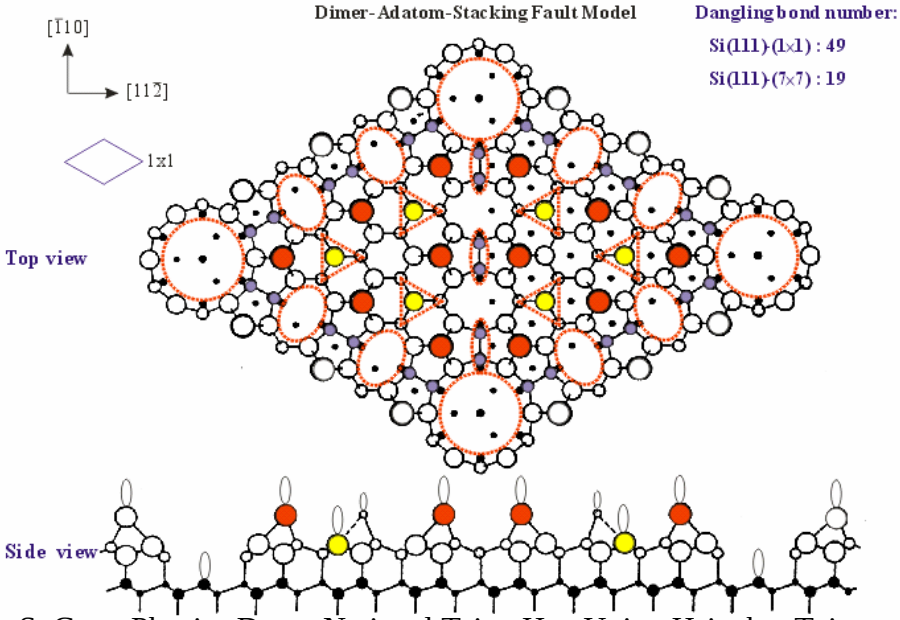

S. Gwo, Physics Dept., National Tsing Hua Univ., Hsinchu, Taiwan

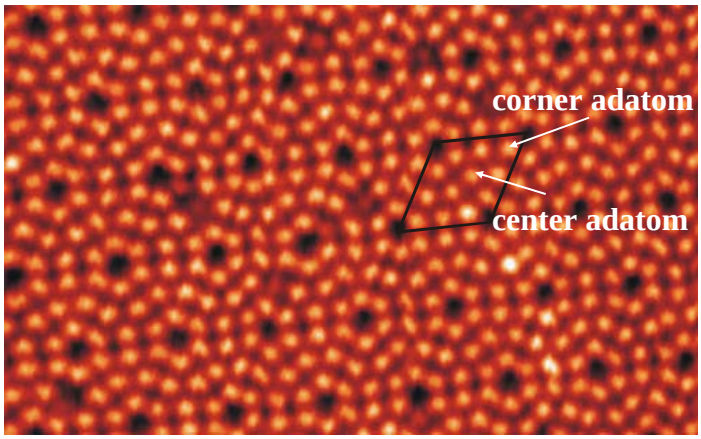

Si(111)-(7 ×7), V_S= 1.6 V, I = 1 nA , Scanning Size = 12.5 nm × 20.5 nm

S. Gwo, Physics Dept., National Tsing Hua Univ., Hsinchu, Taiwan

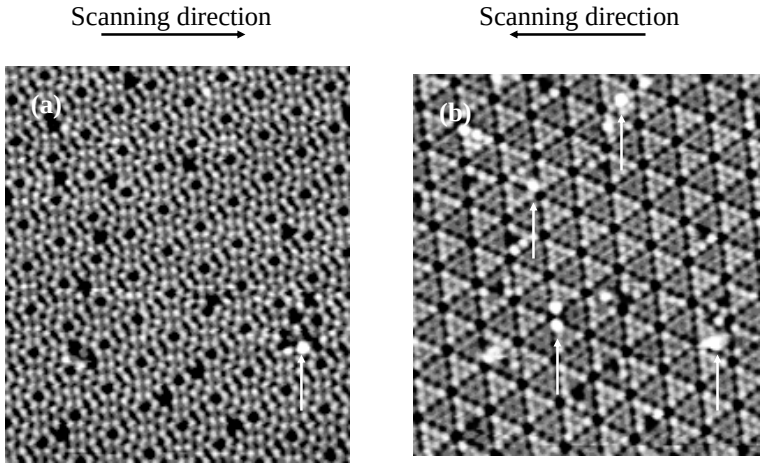

Dual-bias STM Images of Si(111)-(7 ×7)

(a) V_S = 1.5 V, I = 1.5 nA, (b) V_S = -3.5 V, I = 1.5 nA, Scanning Size = 23 nm×25 nm

S. Gwo, Physics Dept., National Tsing Hua Univ., Hsinchu, Taiwan

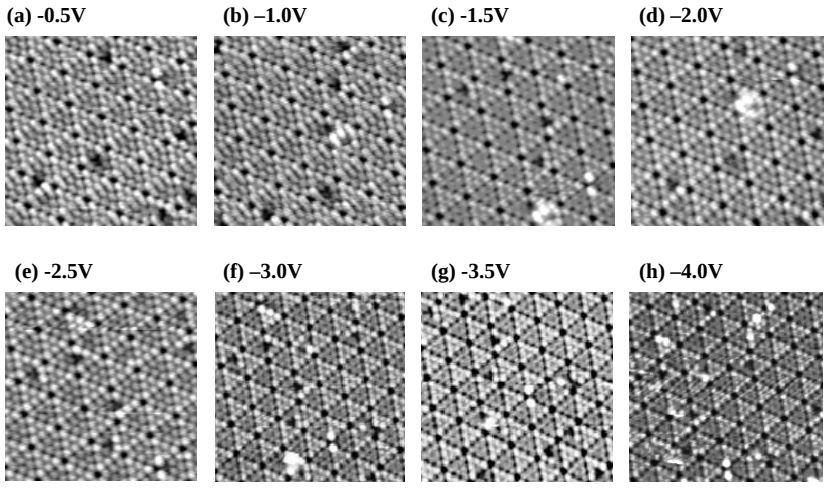

(a)~(h) I=1.5 nA, Scanning Size = 18nm ×18nm

S. Gwo, Physics Dept., National Tsing Hua Univ., Hsinchu, Taiwan

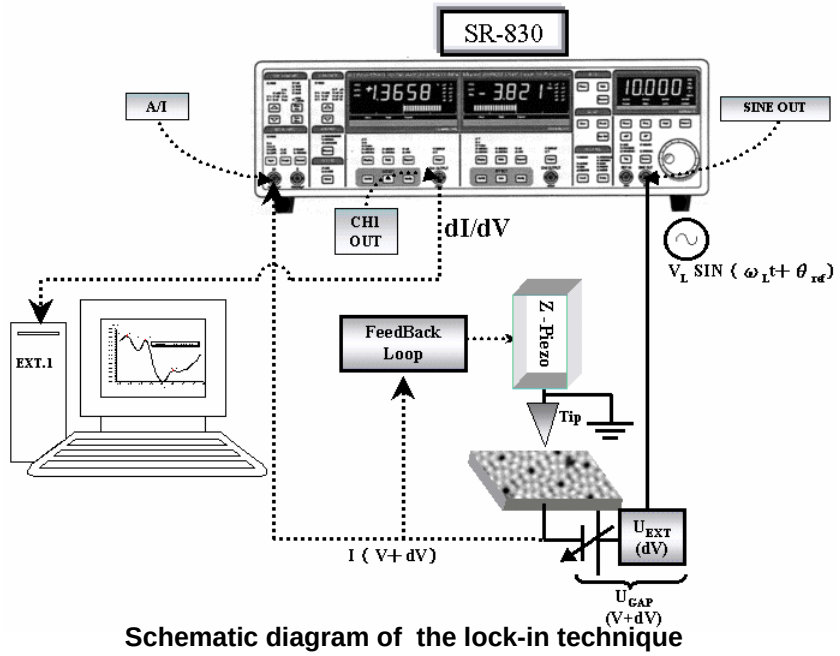

Schematic diagram of the lock-in technique

S. Gwo, Physics Dept., National Tsing Hua Univ., Hsinchu, Taiwan

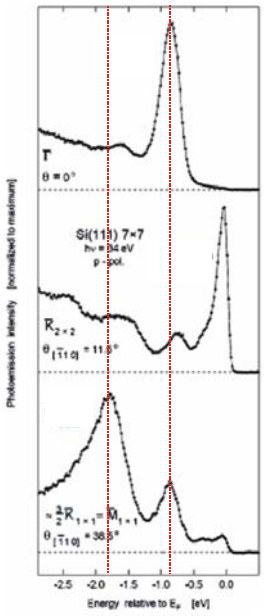

The surface states of the Si(111)-7X7 surface, probed in photoelectron spectra (PES) at various emission angles.

Phys. Rev. B Vol. *61, 10845 (2000)*

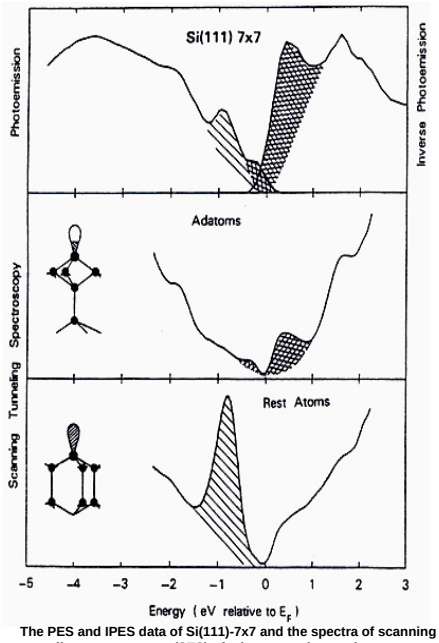

The PES and IPES data of Si(111)-7x7 and the spectra of scanning tunneling spectroscopy (STS) of adatoms and rest adatoms.

Surf. Sci. Rep. Vol. 12,1 (1990)

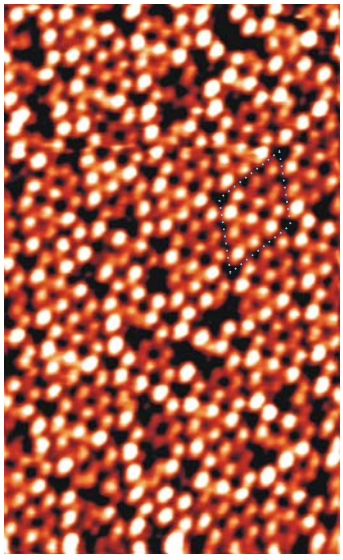

STM filled-state image of the Si(111)-(7x7) surface with V_S=-0.8V and I_t=1.6 nA

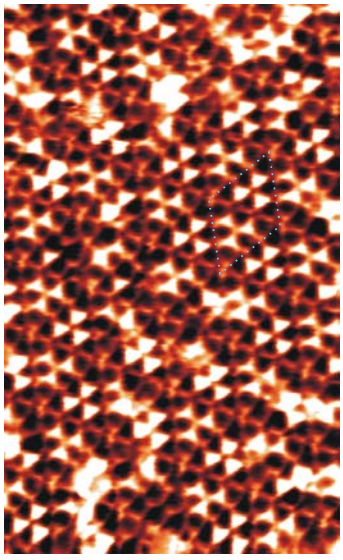

Differential conductivity mapping of the Si(111)-(7x7) surface with V_S=-0.8V and I_t=1.6 nA

S. Gwo, Physics Dept., National Tsing Hua Univ., Hsinchu, Taiwan

Box 1: Fingerprinting individual molecules

The atoms in a molecule vibrate against each other at characteristic frequencies determined by the strength of their chemical bonds. Different vibration modes and their frequencies make up a 'fingerprint', which identifies molecules and pinpoints changes in their bonding owing to chemical reactions. For example, when a molecule is absorbed at a surface, depending on the location or orientation of its absorption site, its vibrational modes may shift in frequency or be suppressed. Knowing these changes is critical to understanding a variety of surface phenomena, such as absorption and release processes, heterogeneous catalysis and epitaxial growth.

Since its invention, the scanning tunnelling microscope (STM) has had the potential to perform site-selective measurements of vibrational spectra of single molecules[32]. This approach was motivated by the success of much earlier experiments in planar metal-oxide tunnel junctions, when the tunnelling conductance was shown to make characteristic jumps at energies corresponding to the characteristic vibrational frequencies of molecules adsorbed at the metal-oxide interfaces in these devices. The underlying principle is that when the energy of the tunnelling electron exceeds that required for exciting a molecular vibrational mode, electrons can tunnel inelastically as well as tunnelling between states of the same energy. This means that they lose energy by causing a molecule near the tunnel junction to vibrate. Sharp steps in the measured conductance at different energies correspond to the onset of inelastic tunnelling processes and provide the fingerprint of the molecular vibrational modes.

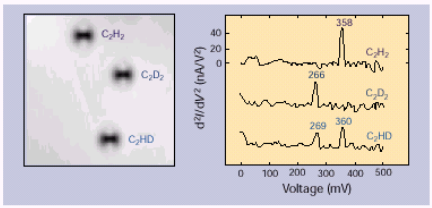

A group at Cornell University, using an STM operating at low temperatures and in ultrahigh vacuum, has succeeded in reproducibly measuring the vibrational spectra of individual molecules[28]. Most impressively, they have used inelastic tunnelling spectroscopy to identify individual molecules by their characteristic vibrational energies[33]. The STM image and inelastic spectra of three similar molecules, C_2H_2, C_2D_2 and C_2HD are shown here. Although STM imaging cannot distinguish between the three molecules, the inelastic tunnelling spectra measured with the tip can reveal their vibrational fingerprints and identify them. The peaks correspond to incremental increases of conductance associated with exciting the C–H and C–D bonds.

A. Y.

Atomic force microscopy

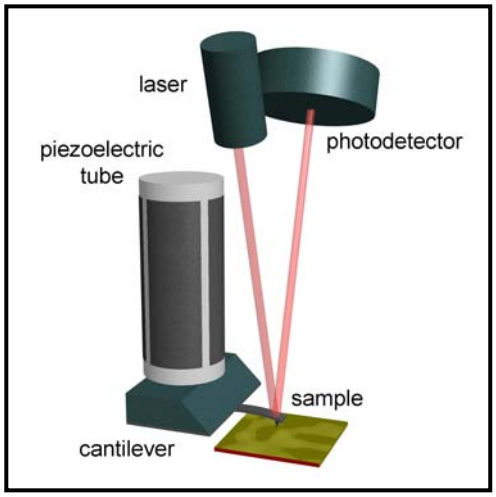

G. Binnig, C. F. Quate, and Ch. Gerber
Phys. Rev. Lett. **56**, 930 (1986).

Post-Processed Silicon Tip

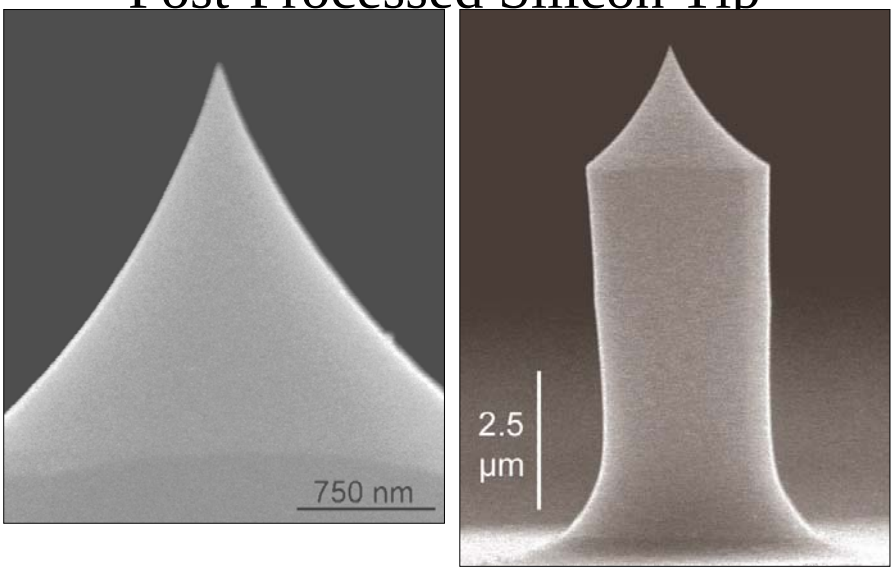

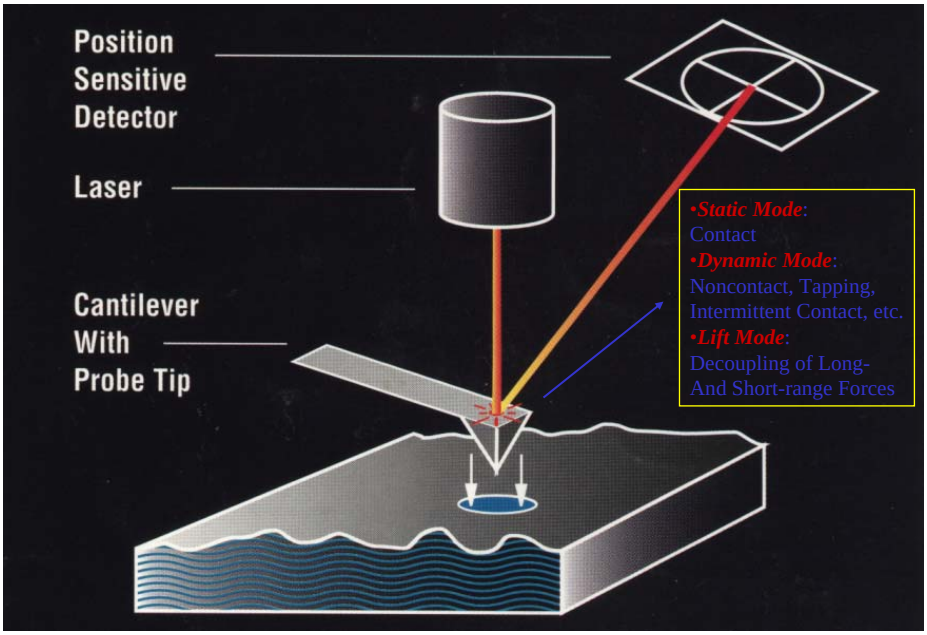

Some Demonstrated Functionalities of AFM

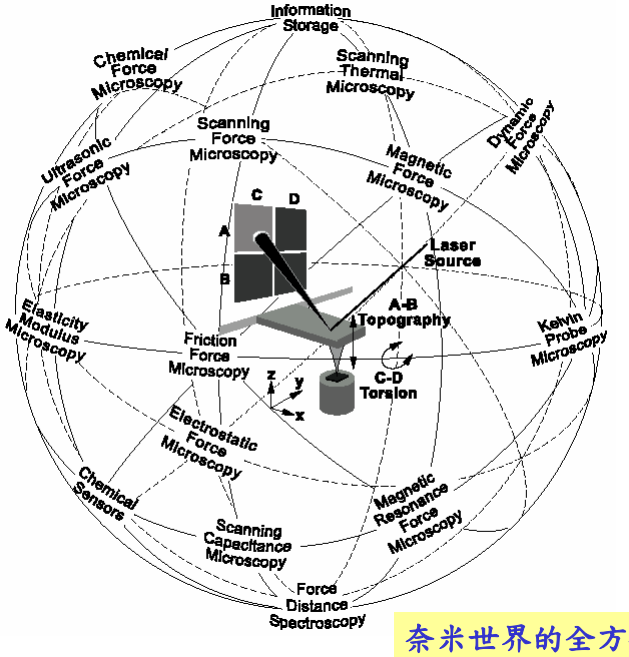

奈米世界的全方位性工具

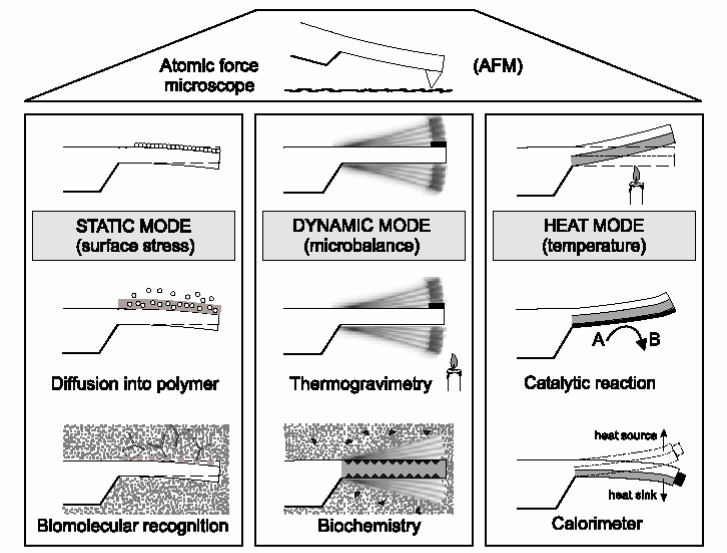

Figure 3. Cantilever sensor operation in the static mode (left), the dynamic mode (middle) and the heat mode (right).
H. P. Lang, M. Hegner, E. Meyer, and Ch. Gerber, *Nanotechnology* Vol. 13, R29-R36 (2002).

APPLIED PHYSICS LETTERS VOLUME 75, NUMBER 16 18 OCTOBER 1999

Nanomachining of (110)-oriented silicon by scanning probe lithography and anisotropic wet etching

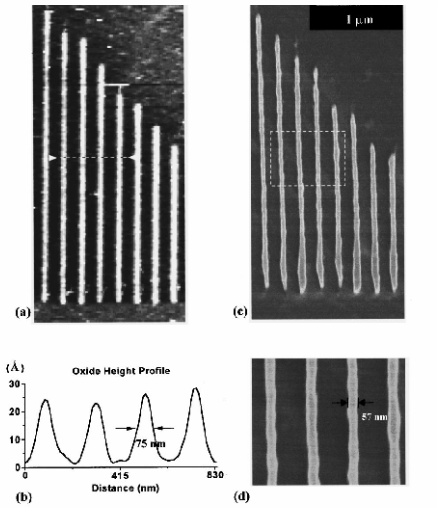

FIG. 2. (a) AFM image of a trapezoidal shape oxide grating patterned by AFM nano-oxidation. (b) AFM topographic height profile along the marked line in (a), showing the protruded height and FWHM of the oxide line. (c) SEM image of the Si grating after pattern transfer by etching in a KOH solution for 60 s. (d) Closeup SEM image of the marked area in (c).

S. Gwo, Physics Dept., National Tsing Hua Univ., Hsinchu, Taiwan

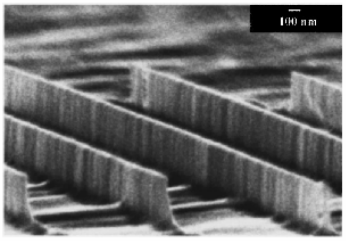

FIG. 3. SEM image of a high aspect ratio Si grating fabricated by AFM nano-oxidation and wet anisotropic etching in a KOH solution for 45 s. The vertical wall height is around 300 nm.

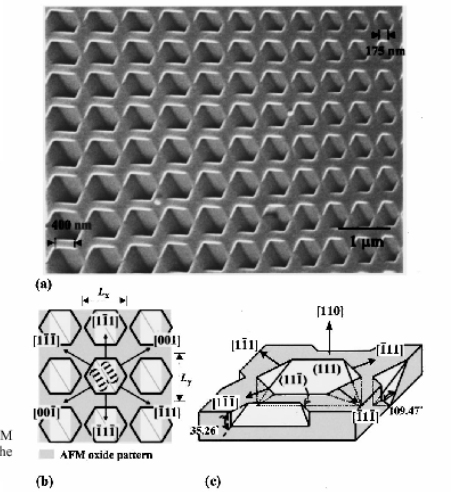

FIG. 4. (a) SEM image of a two-dimensional array of hexagonal pits with varied sizes on the (110)-oriented Si surface. (b) Illustration to indicate crystallographic directions of edges and bottom faces of hexagonal pits. The shadowed area is the oxide grid patterned by AFM nano-oxidation before pattern transfer. (c) Stereoscopic view of a hexagonal pit.

S. Gwo, Physics Dept., National Tsing Hua Univ., Hsinchu, Taiwan

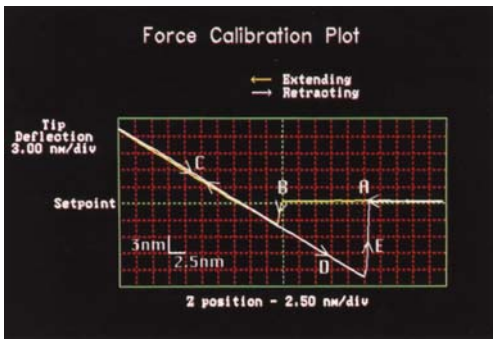

AFM Force Measurement
("Force-Distance Curve")

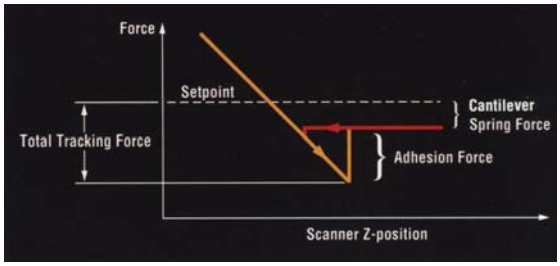

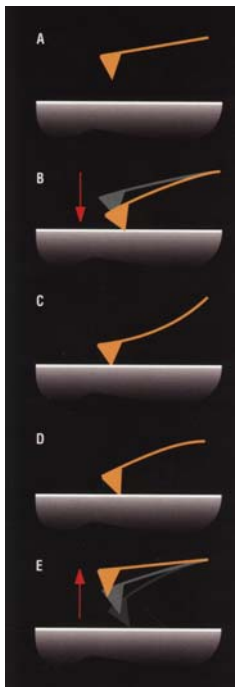

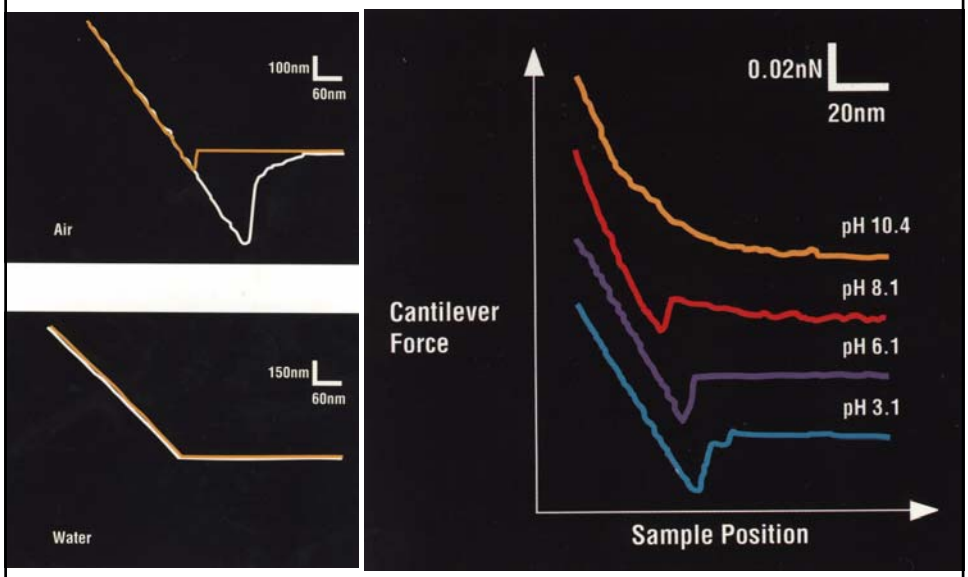

Force measurements between a n AFM tip and a mica surface

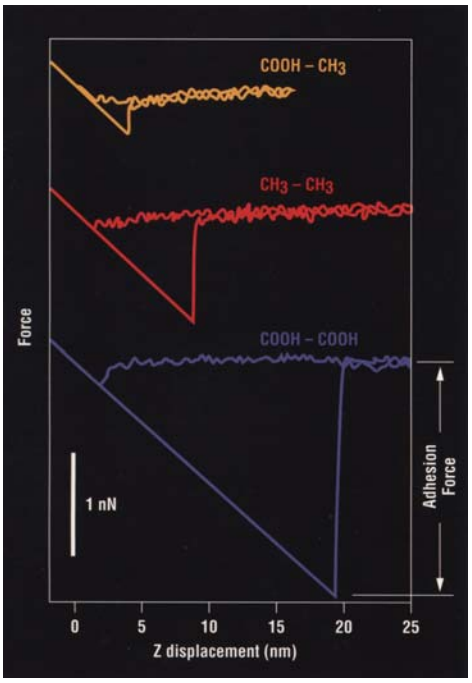

Chemical Force Measurements

Magnetic Force Microscopy MFM

1. Magnetic hard Disk
L: topography by tapping mode
R: MFM by lift mode

2. MFM image of patterned 50-nm permalloy film

3. MFM image of flower Domains in a 60-μm garnet film

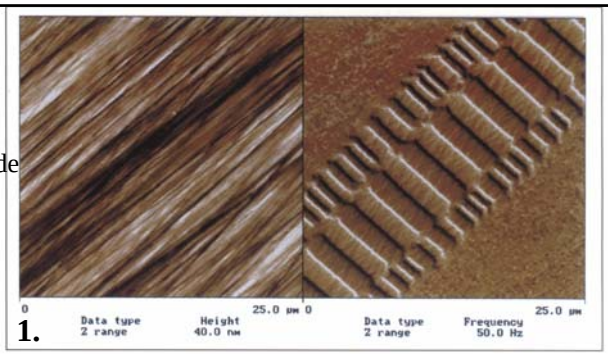

1.

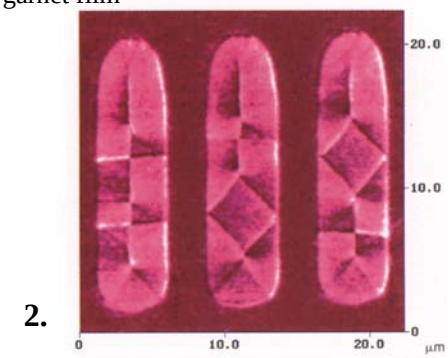

2.

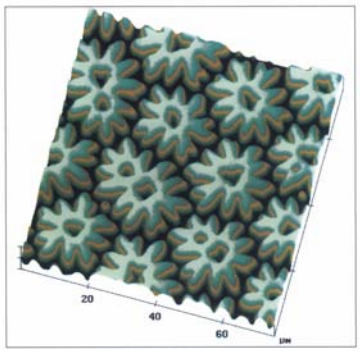

3.

Stephan Fahlbusch*, Sergej Fatikow

University of Kassel, Department of Control and Automation, Faculty of Electrical Engineering, Wilhelmhöher Allee 73, D-34121 Kassel, Germany

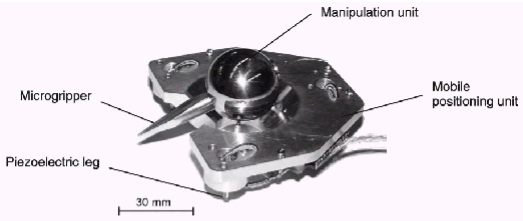

Fig. 2. The SEM-suited microrobot MINIMAN-III.

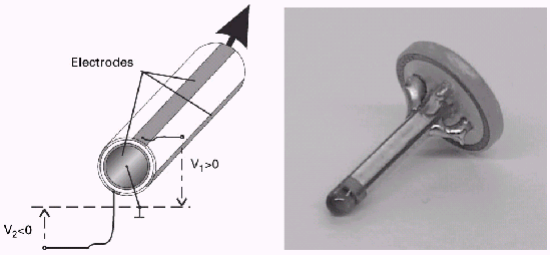

Fig. 3. Piezoelement with segmented electrodes (left), piezoleg with ruby ball (right).

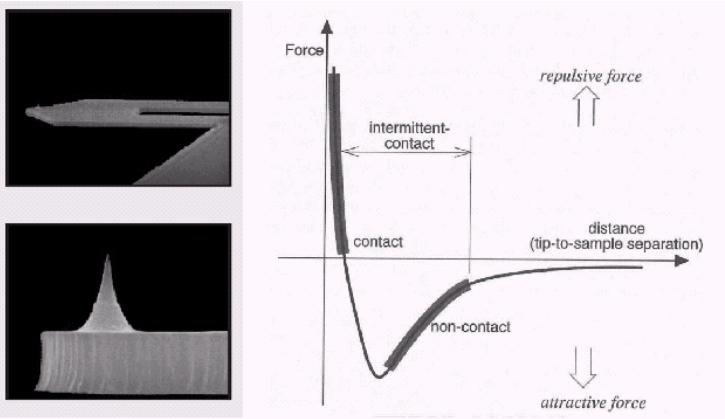

Fig. 13. Piezolever™, ThermoMicroscopes AutoProbe, contact mode (left), interatomic forces (right).

Current difficulties of AFM:

1. Size and shape control of tip
2. Limited detection functionalities
3. Lack of chemical specific information

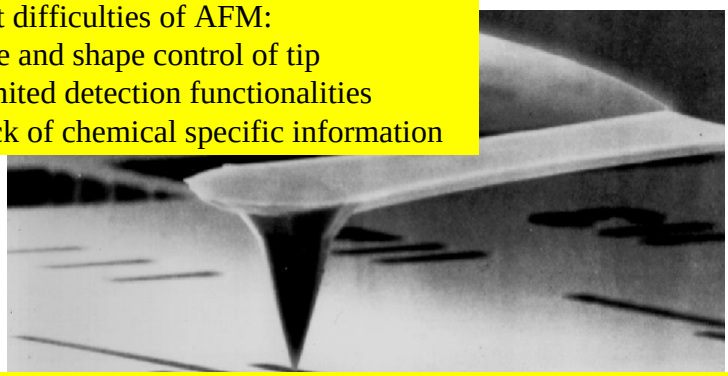

Major drawback of micromachined functional sensors:
Limited spatial resolution determined by the top-down microfabrication

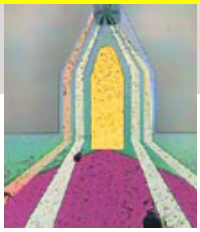

Advantages of carbon nanotube probes for SFM

- Electrically conductive
- Perfectly cylindrical geometry, high aspect ratio
- Mechanically robust with unprecedented elastic properties
- Chemically stable
- Possibility of encapsulate magnetic material inside tube

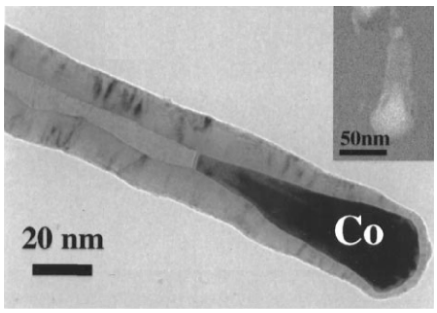

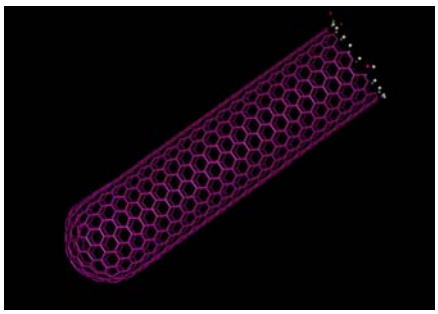

C. Bower *et al*., Appl. Phys. Lett. **77**, 2767 (2000)

S. Gwo (NTHU-Physics)

Field Detection using a Single Carbon Nanotube

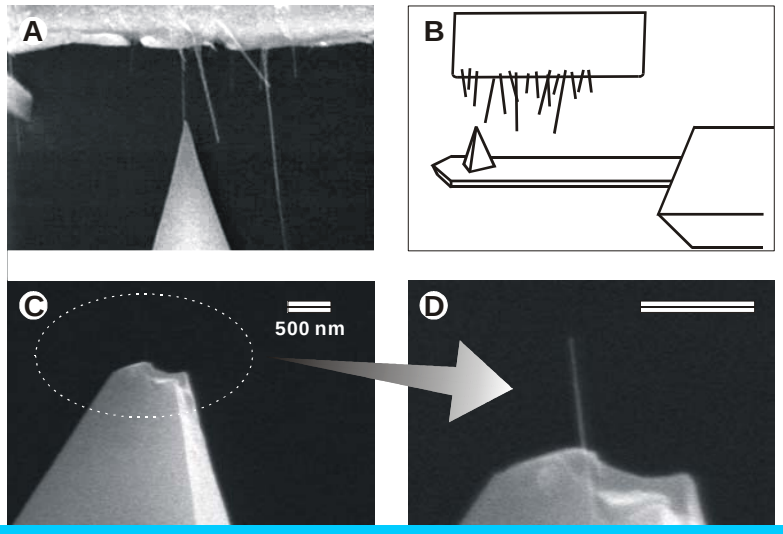

Carbon nanotube:The ultimate probe for imaging long-range forces?

S. Gwo (NTHU-Physics)

EFM Resolution (CNT): better than 5 nm

S. Gwo (NTHU-Physics)

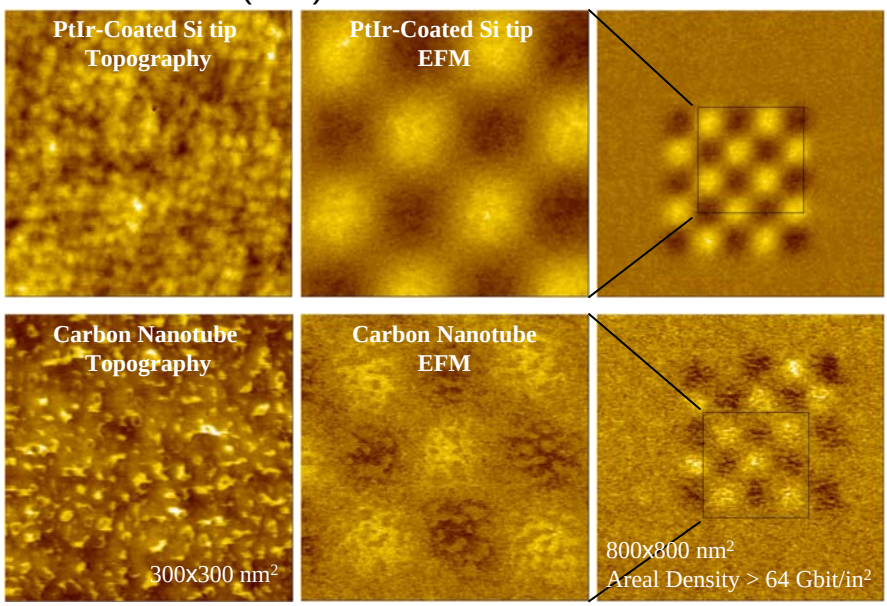

Charging conditions: ±10 V voltage pulses (1-ms pulse-width for PtIr-coated Si tip, 1-s pulse-width for CNT tip)

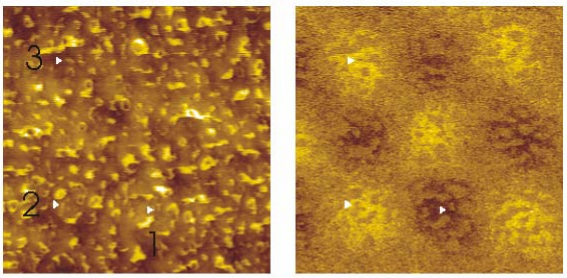

	Topography	EFM
1:	3.1 nm	5.1 nm
2:	4.7 nm	5.9 nm
3:	8.2 nm	6.5 nm

S. Gwo (NTHU-Physics)

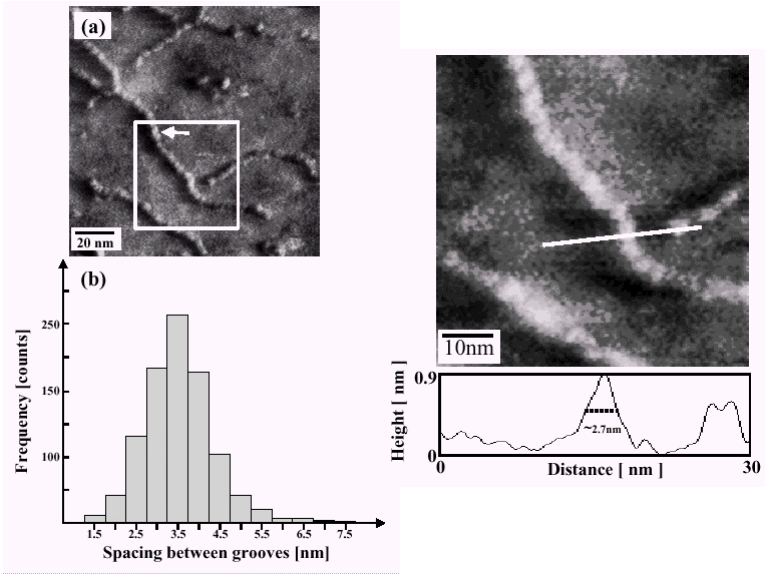

Tokumoto and Nakayama Group

Covalently functionalized nanotubes as nanometre-sized probes in chemistry and biology

Stanislaus S. Wong, Ernesto Joselevich, Adam T. Woolley, Chin Li Cheung & Charles M. Lieber

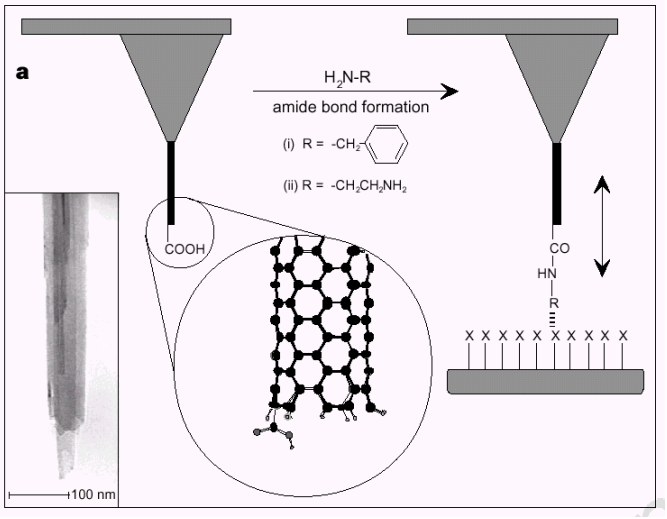

CMOS Compatible Arrays

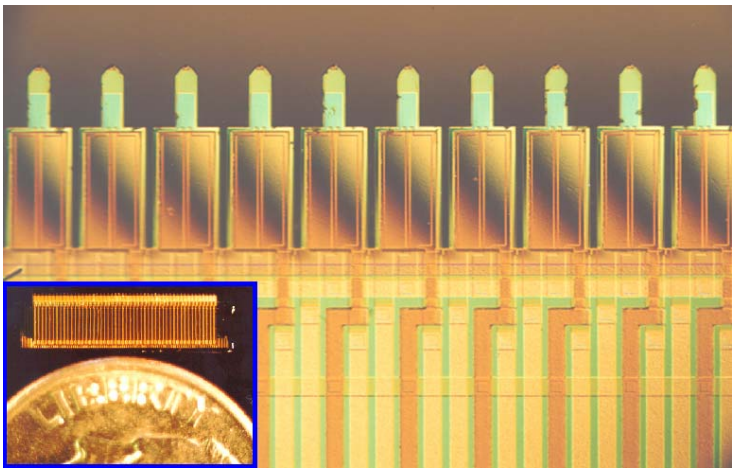

Quate Group, Stanford University

MILLIPEDE
Highly parallel, dense AFM data storage system

"MILLIPEDE" Concept

AFM-based Storage System:

High Data Density But Low Data Rate

⇒ Highly Parallel Operation

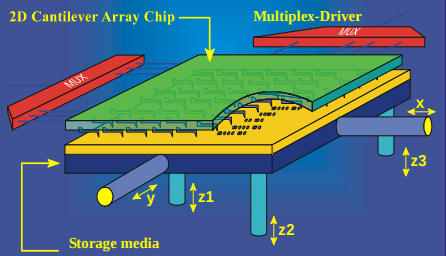

Integrated micromagnetic x/y/z scanner

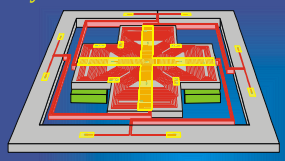

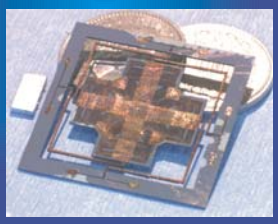

IBM
Zurich Research Laboratory
Micro- and Nanomechanics Team